A Film Fabrication Process on Transparent Substrate using Mask Projection Micro-Stereolithography

Amit S. Jariwala, Fei Ding, Xiayun Zhao, David W. Rosen*

George W. Woodruff School of Mechanical Engineering
Georgia Institute of Technology
Atlanta, Georgia, 30332
*Corresponding author. Tel.: +1 404 894 9668 Email: david.rosen@me.gatech.edu
Reviewed, accepted September 10, 2008

Abstract:

In this study, a Mask Projection Micro-Stereolithography (MPμSLA) process with the ability to cure a film of various thicknesses on transparent substrates is presented. Incident radiation, patterned by a dynamic mask, passes through a transparent substrate to cure photopolymer resin layers that grow progressively from the substrate surface. When compared to existing Stereolithography techniques, this technique eliminates the necessity of recoating, reducing process time and improving accuracy. A film of varying thicknesses can be fabricated on flat or curved transparent substrates. Models of the optical system and resin cure are developed and reported. An existing MPμSLA process planning method is being extended to account for radiation transmission through a substrate. The models are verified using experiments.

1. Introduction

Mask Projection Stereolithography (MPSLA) is an additive fabrication process used to build physical components out of a photopolymer resin. The CAD model of the part to be built is sliced by horizontal planes and the slices are stored as bitmaps. These bitmaps are displayed on a dynamic mask and are imaged onto the photopolymer resin surface. When a bitmap is imaged onto the resin surface, a layer corresponding to the shape of the bitmap gets cured. This layer is coated with a fresh layer of resin by lowering it inside a vat holding the resin and the next layer is cured on top of it. By curing layers one over the other, the entire part is built. This technology has been demonstrated in various papers, like Bertsch et al., (1997), Chatwin, (1998), Monneret et al., (1999), Sun et al.(2005) and Limaye and Rosen, (2007). Commercially available machines include Perfactory® range of machines from EnvisonTec, Germany. The principle behind these machines is similar to that mentioned in the papers above, and sometimes employs more than a single DMD chip to produce multiple parts. One of the interesting aspects of these machines is that the irradiation from the DMD chip passes through a transparent substrate into the resin vat, compared to irradiance from the top of the vat as in conventional micro-SLA processes.

The technologies mentioned above cure parts in a layer by layer fashion on a flat substrate by irradiance from the top of the resin surface. Research has been done on curing parts through transparent substrates, which may enable thin film coating, deposition of micro-channel or modifying a surface of an optical part. Erdmann et al. (2005) had shown the use of mask projection SL through transparent substrates for manufacturing of micro-lens arrays. Mizukami et al. (2002) had proposed the use of curing by laser beam scanning through transparent substrates for manufacture of micro-electrophoretic chips.

In this paper, a film fabrication process on transparent substrate using Mask Projection Micro Stereolithography is introduced. The laser beam patterned by the dynamic mask is projected on the transparent substrate to cure the resin. A process planning method is proposed to control the bitmaps and the time of exposure projected on the dynamic mask for each bitmap. This helps to achieve accurate control over the surface of the cured film. This process can be used to fabricate films on flat or curved substrates.

The experimental setup is discussed in Section 2. Apart from the desired model of the part, the inputs required for process planning include an irradiance model and resin characterization. The irradiance model provides a relationship between the micro-mirrors displayed on the DMD surface and the radiant energy received on the transparent substrate. Resin characterization data relate the response of the photopolymer resin to the irradiated energy by means of a working curve. This working curve helps to determine the energy required to be irradiated on the transparent substrate for a given part geometry. Both the irradiance model and the resin characterization are explained in Section 3.

In Section 4, the overall process planning method is explained. The analytical models for resin characterization and irradiance distribution (obtained in section 3) are fed into a regression model to establish the time of exposure for which each micro-mirror should be displayed in the 'ON' state. In order to optimize the process for displaying the micro-mirrors, a bitmap generation algorithm is used to group the micro-mirrors which need the same time of exposure.

Sample film components are assumed to be designed by the proposed process plan. The bitmaps and the corresponding time of exposure are calculated for these cases using the proposed approach. These simulation results and experimental verification are presented in Section 5.

2. Experimental Setup

The schematic of the MPµSLA system developed is illustrated in Figure 1. The specifications of the system are presented in Table 1. The design of the system can be divided into three modules:

Beam conditioning module: This module consists of a UV laser light source from Omnichrome (now, Melles Griot) (Model # 3074-M-X04). The laser emits 38.5mW

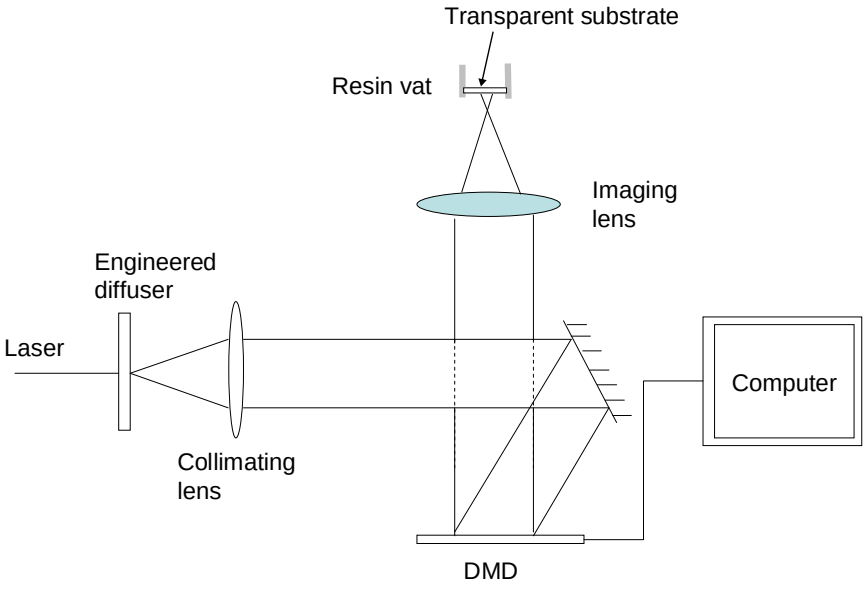

Figure 1 Schematic of the MPSLA system

TEM_{01} at wavelength of 325nm. An Engineered™ Diffuser (micro lens array) is placed right after the laser source to homogenize the beam's intensity profile and enlarge the beam from a diameter of 1.5mm to 50 mm. A UV transmitting Plano-Convex lens with EFL 150.0 mm is used to collimate the light emerging from the diffuser. A UV coated mirror, mounted on a kinematic mount, directs the laser beam on a dynamic mask.

Table 1 Specifications of the Mask Projection SLA system at Georgia Tech

Component	Description	Model/Manufacturer
Laser	Power = 30mW Wavelength = 325nm Beam diameter = 1.5 mm	Omnichrome (Melles Griot)
Engineered Diffuser	Substrate size: 1 x 1", 2mm thick Material: Fused silica Wavelength = 325nm Illumination scatter pattern: Circle Divergence angle: 20° (full-width at 90%) Intensity profile at a plane: Flat-top Uniformity within flat-top region: ± 10%	RPC Photonics Catalog # Customized
Collimating lens	Fused silica Plano convex lens Effective focal length = 150mm Diameter = 50.8mm Radius of surface 1 = 69.0mm Radius of surface 2 = infinity (plane) Lens thickness = 7.8mm Material refractive index = 1.460	Thorlabs Catalog # LA4306-UV
Mirror	Diameter = 25mm. UV Enhanced Aluminum coated	Edmund Optics Catalog # NT45-605
DMD	1024 X 768 array of micromirrors Dimension of micromirror = 12.65µm square. Spacing between mirrors = 1µm	Texas Instruments. Distributed by Prod. Sys Inc.
Imaging Lens	Fused silica Plano convex lens Effective focal length = 75mm Diameter = 25.4mm Radius of surface 1 = 34.5mm Radius of surface 2 = infinity (plane) Lens thickness = 6.7mm Material refractive index = 1.460	Edmund Optics Catalog # LA 4725-UV
Photopolymer resin	E_c, D_p determined experimentally	Vantico Huntsman SL-5510

Imaging module: The Imaging module consists of a dynamic mask, the Digital Micromirror Device, (DMD™), an imaging lens (a UV transmitting Plano-Convex lens with an EFL of 75.0 mm). The DMD is an array of individually addressable, bi stable micro mirrors, which can be selectively oriented, to display any bitmap. Every pixel on the bitmap controls one and only one micromirror on the DMD. The micromirrors are 12.65 µm square and the spacing between adjacent micromirrors is 1µm. The micromirrors in their neutral state are parallel to the DMD chip. In its "ON" state, a micromirror swivels about its diagonal by 12° in one direction and in the "OFF" state, swivels by the same amount in the opposite direction. The DMD™ is a product of Texas Instruments and was sold by Productivity Systems Incorporated (PSI™). The bitmap displayed on the DMD serves as the object for the imaging system. The bitmap is imaged onto the substrate by the imaging lens. The DMD is mounted parallel to the horizontal plane. The

object distance, as measured from the center of the pattern to the mid plane of the imaging lens, was 152 mm and the image distance, measured from the mid plane of the imaging lens to the resin surface, was 132 mm. The radius of curvature of the Plano-Convex imaging lens is 34.25 mm and the thickness of the lens is 4.4 mm. The refractive index of the lens material is 1.460 (air). The above-mentioned data was used in the ray-tracing algorithm, described in the section "Irradiance Model".

Resin vat: The resin vat is a rectangular container with the base made of a transparent glass slide. This glass slide acts as the substrate over which the film is cured.

3. Analytical modeling

In this section, the irradiance model is presented in which the irradiation produced by individual micromirrors on the DMD mask onto the resin surface is computed by first order ray tracing. The working curve for the resin is characterized on this setup using experiments. This working curve is used further as an input for process planning.

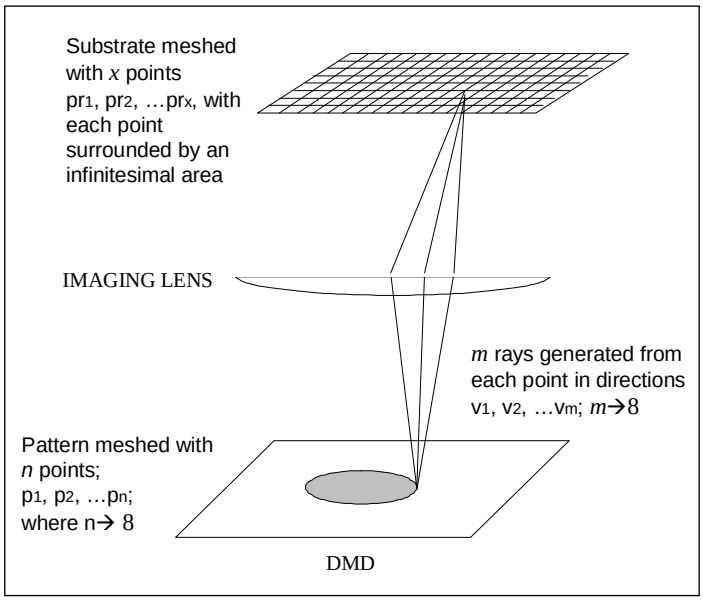

Figure 2 Schematic of ray tracing algorithm

Irradiance model

Irradiance Model models the irradiance received by the resin in terms of the process parameters. The irradiance distribution on the resin depends upon the power distribution across the light beam incident on the bitmap and upon the optical aberrations caused by the imaging lens. The ray tracing algorithm is adopted from Limaye & Rosen (2007). Figure 2 shows the schematic of the ray tracing algorithm for projection of light rays from DMD onto flat substrate.

The irradiance distribution across the beam incident on the DMD is assumed to be uniform and the value is measured using a radiometer. This irradiance is one of the inputs to the Irradiance model.

The Irradiance, $H(pr_i)$ at a point in the resin can be given by:

$$H(pr_i) = c \sum_{j=1}^{n} \sum_{k=1}^{m} \delta(p_j, v_k, pr_i) \qquad (1)$$

where c is a constant. δ is a function introduced to evaluate whether a particular ray will strike an infinitesimal area centered on a given point on the resin or not. p_j corresponds to the number of points: p_1, $p_{2,\ldots}p_n$, where n→ ∞ on the DMD. $\boldsymbol{v}_k$ (v_1, v_2, …v_m, where m→ ∞) represents the direction vector in which the rays are emitted from the point on the DMD and p_{ri} (pr_1, $pr_{2,\ldots}$, pr_x, where x→ ∞) is a point on the substrate. Since a collimating lens is used in conjunction with the diffuser, the light beam incident on the DMD is fairly collimated with a divergence angle of less than 1 degree. To take into account the effect of the minor divergence, a cone of rays is emitted from each pattern point.

Resin Characterization

For a point (pr_i), exposure $E(pr_i)$ is given by $E(pr_i) = E(pr_i) * t$, where t is the exposure time at this point. According to a threshold model proposed by Jacobs (1992), a resin point is cured if and only if the exposure received by this point is greater than the threshold exposure of polymerization (E_c).

The variation in exposure with depth in the resin follows the Beer Lambert's law of absorption. So, the exposure at a height *z* in the resin is given as:

$$E(pr_i, z) = E(pr_i)e^{-z/D_p} \tag{2}$$

where D_p is the depth of penetration of the resin. Again, if $E(pr_i, z) \geq E_c$, the resin will cure at that point. So, the depth to which the resin will cure at a point pr_i receiving irradiance $H(pr_i)$, when exposed to irradiation for a time t, is given by:

$$C_d(pr_i) = D_p \ln(H(pr_i)t / E_c) \tag{3}$$

The model in Eq. (3) is based on an assumption that the attenuation of radiation through a cured layer is the same as that through uncured resin. It does not count the effects of radiation through a cured part, which is in solid phase. Limaye & Rosen (2007) have observed experimentally that the attenuation through a cured layer is significantly less than that through the liquid resin. Thus, the depth of penetration for a cured layer D_{pS} is expected to be different from that for the liquid resin D_{pL}. The layer cure model developed by Limaye & Rosen (2007) by modeling the layer curing as a transient phenomenon is given below,

$$dz = D_{pL} \ln[1 + \frac{dE \cdot \exp(-z / D_{pS})}{E_c}] \tag{4}$$

After applying Taylor series expansion and omitting the higher order terms, Eq. (4) can be further simplified as

$$dz \approx D_{pL} \cdot \frac{dE \cdot \exp(-z / D_{pS})}{E_c} \tag{5}$$

The layer curing model is obtained after solving the ordinary differential equation above,

$$z \approx D_{pS} \cdot \ln(\frac{D_{pL}}{D_{pS}} \cdot \frac{E}{E_c} + 1 - \frac{D_{pL}}{D_{pS}}) \tag{6}$$

Through experimentation, the resin cure characteristics were obtained to provide a relationship between the amount of exposure and the curing depth. The resin used with the MPμSLA system under consideration is the Vantico Huntsman SL-5510 resin. The values of E_c and D_p have been specified by the resin manufacturer to be 8.9 mJ/cm^2 and 0.122 mm respectively. Research on MPμSLA systems has shown that the experimentally observed values of E_c and D_p differ from their values specified by the manufacturer (Bertsch et al., 2000, Farsari et al., 2000, Hadipoespito, 2003). So, the resin needs to be characterized experimentally to determine the values of E_c and D_p. Fig. 3 shows the working curve for the resin obtained by our proposed setup.

The following experiments were performed to determine the values of E_c and D_p. A thin film is cured on a flat glass substrate by exposing it to radiation for different time durations. By varying the time of exposure, the radiant energy received by the film is varied. The thickness of the cured film is plotted against the exposure received by the film as shown in Figure 3. From the plot, the value of E_c, D_{pS} and D_{pL} are found to be 4.0mJ/cm^2, 0.015mm and 0.011mm, respectively, which are lower than the manufacturer's specified value.

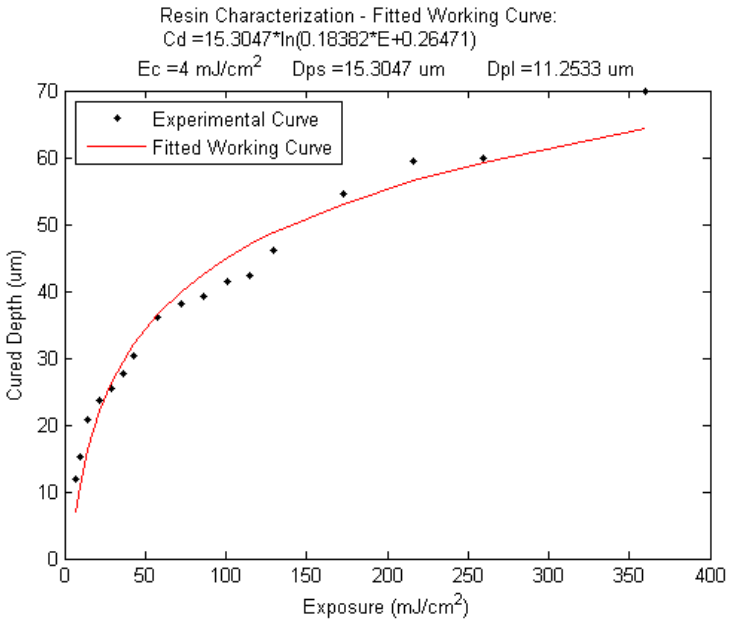

Figure 3 Working curve of Huntsman 5510 resin with the MPµSLA system

4. Process planning method

A process planning method is formulated to generate the bitmaps to be displayed on the DMD and the times for which they should be imaged onto the resin to cure a thick film with the required dimensions. A bitmap displayed on the DMD is nothing but a cluster of micromirrors oriented in a particular direction. Using the Irradiance Model, the correspondence between the location of an "ON" micromirror on the DMD and the locations of pixels irradiated by it on the resin can be established. By applying a regression model, the time for which each micromirror needs to be imaged onto the resin to cure a certain part can be computed. The micromirrors with similar times of exposure are grouped together to generate multiple bitmaps. Thus, the input to the process planning method is the three dimensional

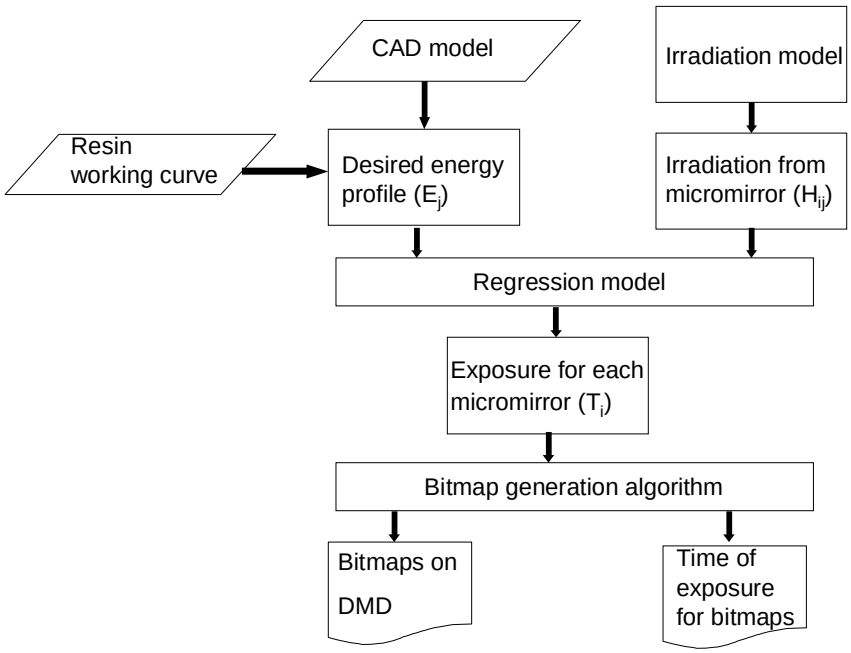

Figure 4 Flow-chart of proposed process plan

geometric profile of the part to be cured on a transparent flat/curved substrate and the outputs are the bitmaps to be displayed on the DMD and the times of exposure (TOE) for which they should be imaged onto the resin surface. The schematic of the process plan is explained in Fig. 4.

The detailed idea of the proposed process planning method could be explained in the context of Figure 5. Fig. 5 shows the CAD model representation of a film to be cured on the substrate. The base surface area of this CAD model is discretized into a number of square pixels with average height, Z_{ij}. Each column corresponds to one pixel on the substrate. The energy required to cure the height, Z_{ij} along this column can be obtained from the resin characterization curve as, E_{ij}. The energy irradiated on the pixels of the resin is a result of irradiance produced by the micromirrors and the time for which the micromirrors are switched "ON". For each of the pixels on the resin, the objective is to minimize the deviation of the exposure received from the micromirrors and the required energy, E_{ij}. The time of exposure for each micromirror can be obtained by satisfying the least squares minimization.

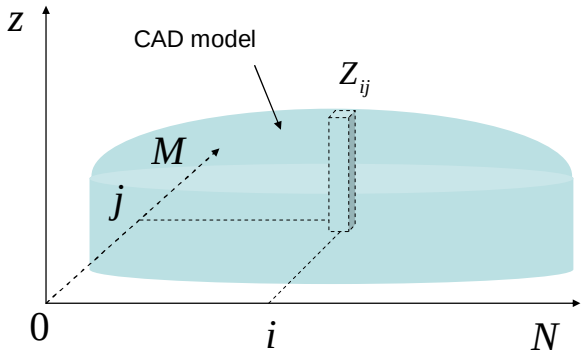

Figure 5 Stereolithography parameter estimation formulation example

Regression Model: For the sake of this study, irradiance produced by a micromirror on a pixel in resin is represented as H_{ijkl}, where ij corresponds to the pixels on the substrate (400 x 400 pixels) and kl corresponds to the number of micromirrors (300 x 300 mirrors) on the DMD mask. Thus, H_{ijkl} represents the irradiance on the $(i \text{ x } j)^{\text{th}}$ pixel of the flat substrate caused by the $(k \text{ x } l)^{\text{th}}$ micromirror on the DMD mask. H_{ijkl} could be obtained from the irradiance model in Section 3.

The parameter optimization algorithm proposed by Sager & Rosen (2008) is adopted to develop the regression model. The exposure at each $(i \text{ x } j)^{\text{th}}$ pixel on the resin surface is, $H_{ijkl} * T_{kl}$, where T_{kl} is the time of exposure of each micromirror. If the exposure required at each pixel is E_{ij} then, the least-squares fitting problem can be formulated as follows,

Given: Geometry of the part $z = G(x, y)$.

Resin properties: penetration depths (for solid and liquid), D_p, critical exposure, E_c.

Irradiance on the $(i \text{ x } j)^{\text{th}}$ pixel on the resin surface by $(k \text{ x } l)^{\text{th}}$ micromirror, H_{ijkl} (Obtained from the Irradiance Model).

Find: Exposure time for every micromirror: T_{kl}, k = 1, 2 …P (number of elements on DMD along x-direction), l = 1, 2 …Q (number of elements on DMD along y-direction).

Minimize: $\min S = \sum_{i=1}^{N}\sum_{j=1}^{M}\left(E_{ij} - \tilde{E}_{ij}\right)^2 = \sum_{i=1}^{N}\sum_{j=1}^{M}\left(E_{ij} - \sum_{k=1}^{P}\sum_{l=1}^{Q} H_{ijkl} * \tilde{T}_{kl}\right)$ (7)

Constraints: $T_{kl} \geq 0$ (8)

Bitmap Generation: After the time of exposure for each micromirror, T_{kl}, is obtained and a micromirror grouping algorithm is applied. The set of T_{kl} values is divided into groups, in which the values for times of exposure are similar. The average time of exposure for each group, T^i, i = 1, 2, 3, … N (number of groups), is assigned as times of exposure for all the micormirrors in this group. In order to ensure that each pixel on the substrate get continuous curing till desired thickness, the following bitmap generation method is developed.

1) $T_1 = \left\{T_1^i \middle| T_1^i = T^i\right\}, i = 1,2,3,...,N. \quad t_1 = \min(T_1)$ (9)

Bitmap pattern 1: P_1 =group of micromirrors with $T_1^i \geq t_1$

2) $T_2 = \left\{T_2^i \middle| T_2^i = T_1^i - t_1\right\} \quad t_2 = \min(T_2)$ (10)

Bitmap pattern 2: P_2 =group of micromirrors with $T_2^i \geq t_2$

. . .

K) $T_k = \left\{T_k^i \middle| T_k^i = T_{k-1}^i - t_{k-1}\right\}, t_k = \min(T_k)$ (11)

Bitmap pattern K : P_K =group of micromirrors with $T_k^i \geq t_k$

. . .

Display each bitmap pattern P_K with time duration of t_K .

In this paper, the bitmap generation process was done manually. An automatic method using kmeans clustering algorithm is under development.

5. Results and Discussions

In order to experimentally verify the process planning method in the MPμSLA system, three cases are studied.

Case 1: The CAD model for Case 1 is shown in Fig. 6(a). The part is composed of two square blocks with a step height of 30 μm. The front-side view of the part is shown in Figure 6(b). To reduce the computation time, a 2D profile in Fig. 6(b), which can be extruded along the *y* axis to yield the 3D part, is considered in the regression model. From the working curve in Figure 3, the desired exposure profile is plotted in Figure 6(c).

The irradiation on the substrate was obtained for every micromirror on the DMD using the irradiance model. Figure 7 shows the irradiance distributions on the substrate corresponding to the micromirror at the DMD center and the micromirror at the middle of an edge. In Figure 7(a), the center area with most intensive irradiation is 10*10 μm. The size of surrounding area is 20 μm with less than half of the irradiation at the center. For the edge micromirror shown in

Figure 7(b), the area with the most intensive irradiation is 10*20 µm. However, because of the offset of the micromirror to the optical axis of the system, more blur area appears on the irradiation area from the edge micromirror than that from the center micromirror.

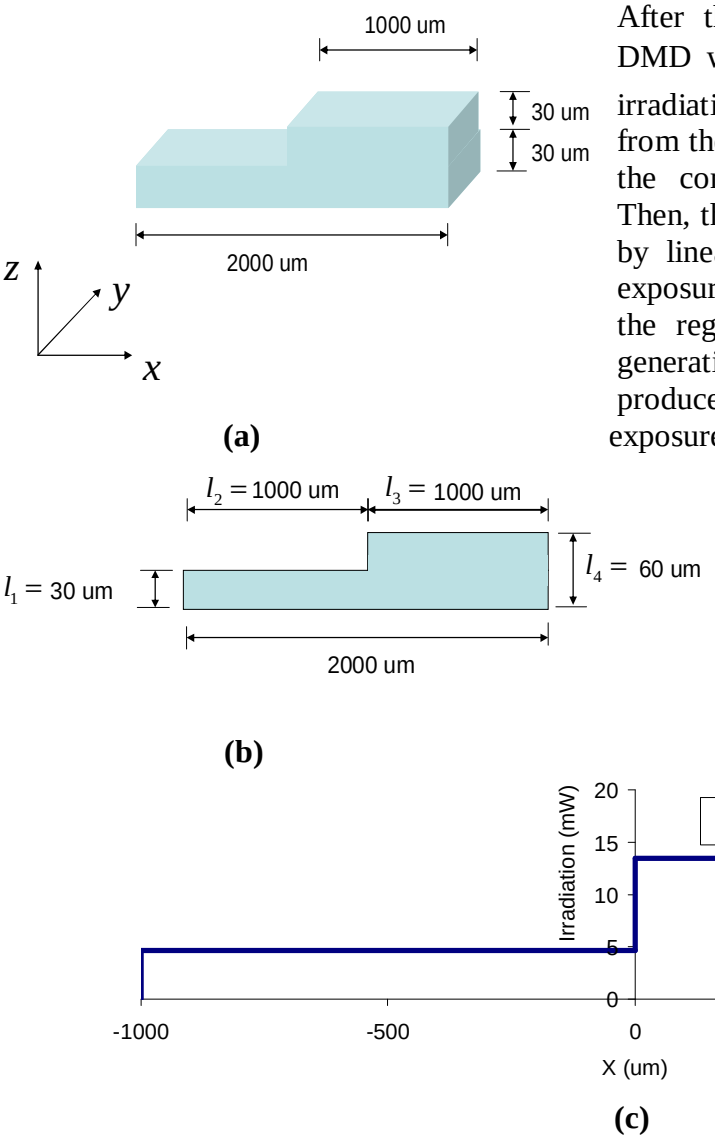

Figure 6 (a) The CAD model (desired cured shape) for Case 1; (b) The front-side view of the desired cured shape for Case 1; (c) The corresponding desired irradiation profile for Case 1.

After the irradiation for each micromirror on DMD was generated, H_{ijkl}, the contribution of irradiation on the (i x j) th pixel on the substrate from the (k x l)th micromirror was obtained from the corresponding irradiation profile directly. Then, the regression model in Eq. (7) was solved by linear least squares method to the time of exposure for every individual micromirror. After the regression model was solved, the bitmap generation algorithm (Eq. 8-10) was applied to produce the sequence of bitmaps and the time of exposure for each bitmap. Figure 8 shows the two bitmaps which were displayed on the DMD for the specified time in order to cure the desired shape as shown in Figure 6(a) for Case 1. Figure 8(a) is the first bitmap displayed on DMD. After the first bitmap was displayed on DMD for 47 seconds, it was replaced by the second bitmap shown in Figure 8(b). The second bitmap was displayed on the DMD for 111 seconds to finish the curing process.

The cured shape from the experiments for Case 1 is shown in Figure 9. The area enclosed by the blue lines is the cured part. Since the film is cured on a transparent substrate, measurements for thickness are performed from the base of the glass substrate. The hazy images on the other side of the measured datum are from the reflections produced from the transparent substrate. Comparison of the cured part and the desired shape in Fig. 6(b) is shown in Table 2. The cured shape from the experiment agrees with the shape from the simulations. However, the

generated surface is rough in appearance and needs further improvement in the setup to enable generation of smoother surfaces.

Table 2 Comparison on dimensions of desired part and part from experiments

Dimension	Desired (um)	Cured (um)	Percent Error
l_1	30	32	6.7%
l_2	1000	910	9.0%
l_3	1000	960	4.0%
l_4	60	54	10%

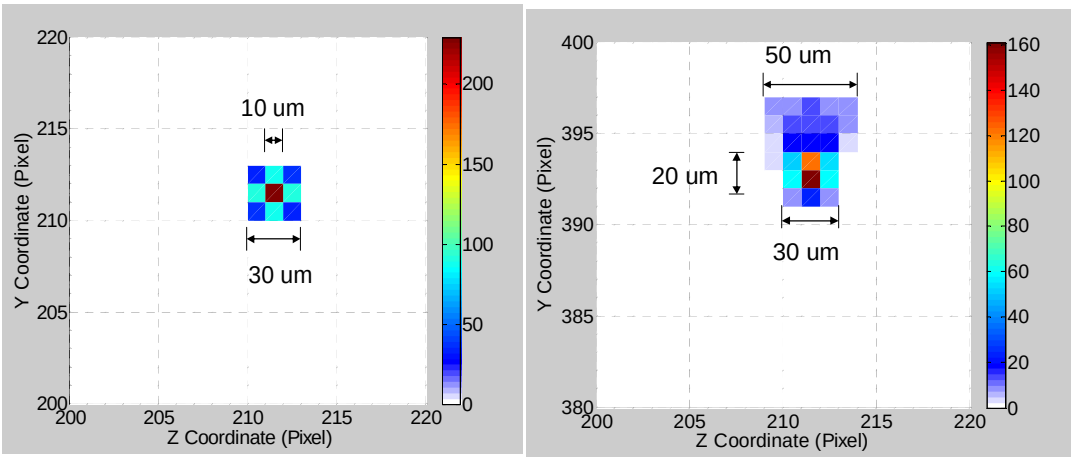

(a) **(b)**

Figure 7 (a) Irradiation on the flat substrate from center micromirror (151,151); (b) Irradiation on the flat substrate from the edge micromirror (151,301).

(a) 1st bitmap (T=47s) **(b) 2nd bitmap (T=111s)**

Figure 8 Bitmaps displayed on DMD for Case 1

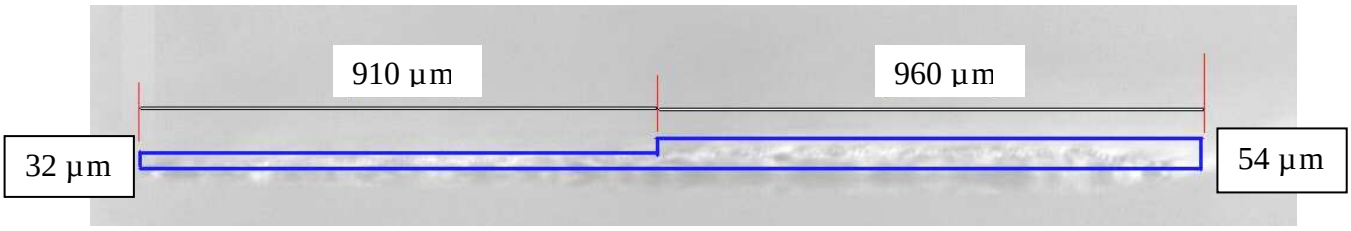

Figure 9 Cured shape from experiments for Case 1.

Case 2: Similarly, Figure 10(a) shows the CAD model for Case 2. The 2D profile of the CAD model is shown in Figure 10(b). After applying the regression model, the bitmap series

displayed on the DMD are listed in Fig. 11. Figure 12 shows the cured part from the experiments. The straight line shows the boundary of the cured part.

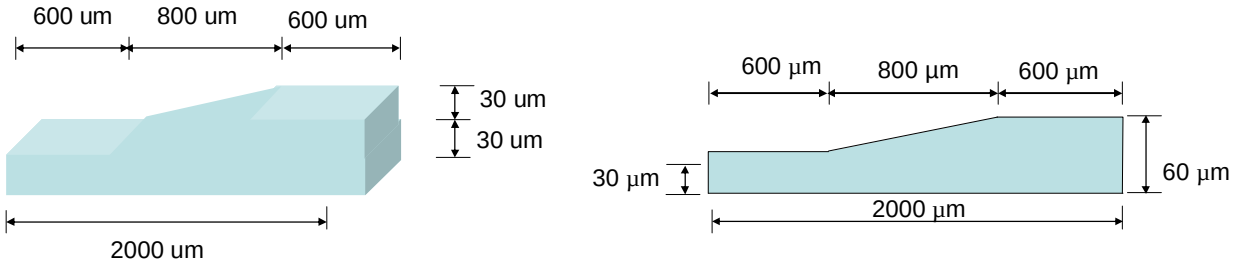

(a) **(b)**

Figure 10 (a) The CAD model (desired cured shape) for Case 2; (b) Front-side view of the desired cured shape for Case 2.

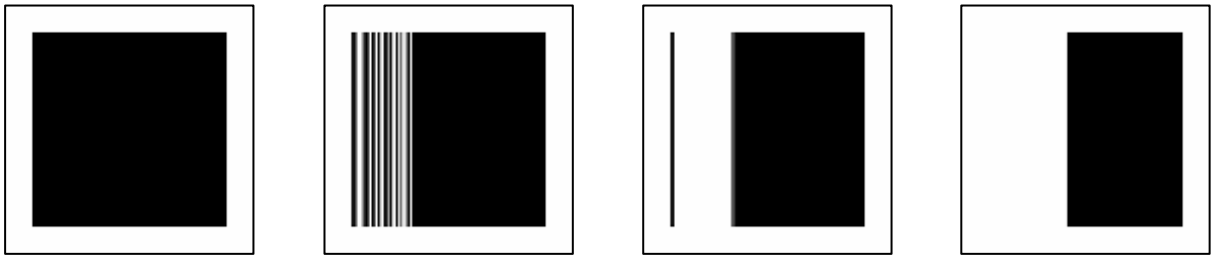

(a) 1st bitmap (T=177s) **(b) 2nd bitmap (T=21s)** **(c) 3rd bitmap (T=62s)** **(d) 4th bitmap (T=122s)**

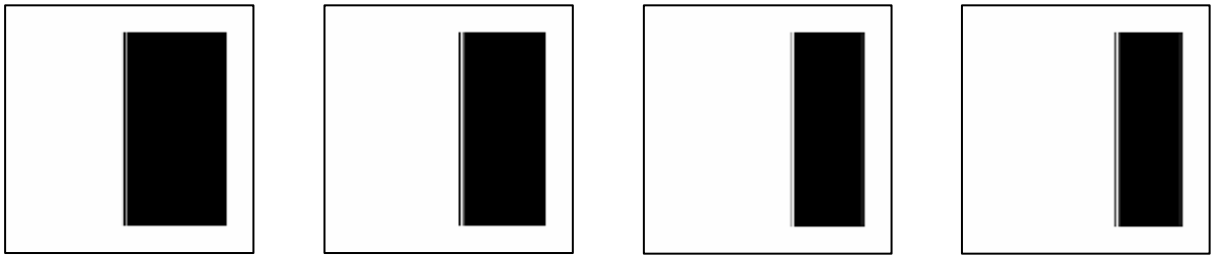

(e) 5th bitmap (T=193s) **(f) 6th bitmap (T=231s)** **(g) 7th bitmap (T=186s)** **(h) 8th bitmap (T=329s)**

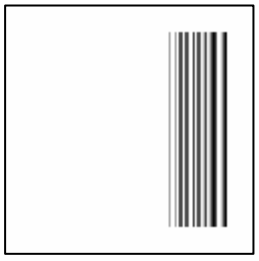

(i) 9th bitmap (T=206s)

Figure 11 Bitmaps displayed on DMD for Case 2

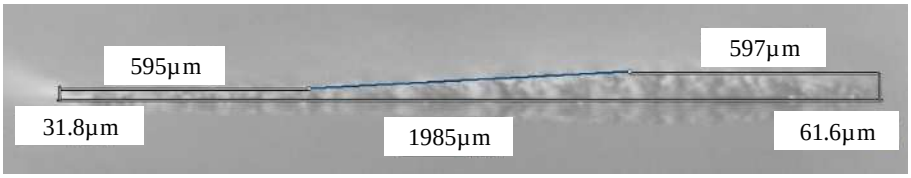

Figure 12 Cured shape from experiments for Case 2.

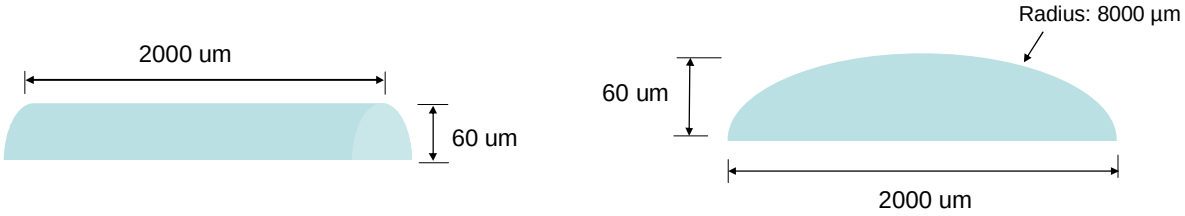

(a) **(b)**

Figure 13 CAD model (desired cured shape) for Case 3; (b) Front-side view of the desired cured shape for Case 3.

Case 3: Figure 13 shows the desired shape for the third example. Figures 14 and 15 show the bitmaps series for the DMD and the experimental results, respectively.

All the dimensional errors in Case 2 and Case 3 are less than 10%.

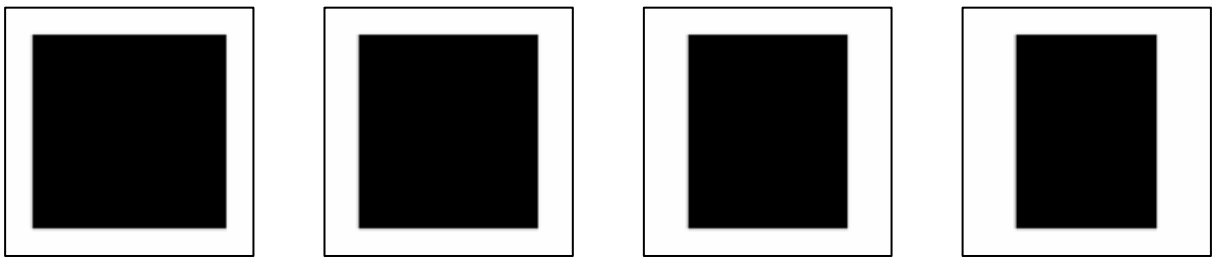

(a) 1st bitmap (T=39s) **(b) 2nd bitmap (T=36s)** **(c) 3rd bitmap (T=66s)** **(d) 4th bitmap (T=103s)**

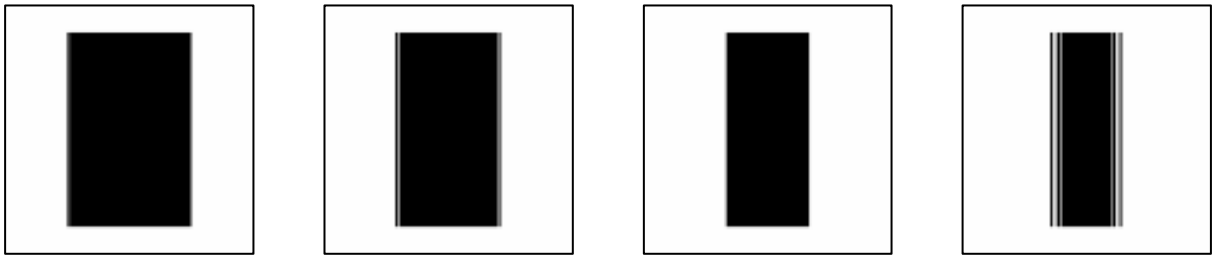

(e) 5th bitmap (T=149s) **(f) 6th bitmap (T=189s)** **(g) 7th bitmap (T=208s)** **(h) 8th bitmap (T=215s)**

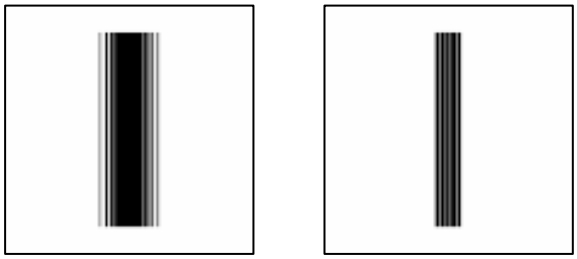

(i) 9th bitmap (T=181s) **(j) 10th bitmap (T=213s)**

Figure 14 Bitmaps displayed on DMD for Case 3

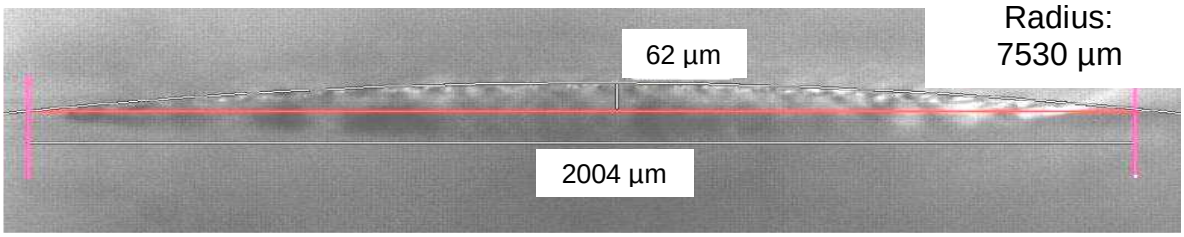

Figure 15 Cured shape from experiments for Case 3.

5. Conclusions

In this paper, Mask Projection Stereolithography was demonstrated as an applicable process for fabrication of films of varying thickness on transparent substrates. A detailed process plan based on the Energy Threshold model was presented. The proposed process planning method provided the bitmap sequence and time of exposure for each bitmap to be displayed on the DMD mask.

The results from the process planning method enabled curing of a film with the desired profile. However, the experimental results suggest the necessity to further improve the process planning method by incorporating additional constraints in the regression model like, resin cure kinetics, oxygen inhibition effect, shrinkage, etc. These factors would be incorporated in our future work to gain a better control over the generated cure profile of the film. Extension of the proposed fabrication process for different resins shall be studied for increasing the potential applications of this process.

6. References

Bertsch A., Zissi S., Jezequel J., Corbel S., Andre J. (1997) "Microstereolithography using liquid crystal display as dynamic mask-generator", *Microsystems Technologies, Vol 3 No 2, pp. 42-47.*

Chatwin C., Farsari M., Huang S., Heywood M., Birch P., Young R., Richardson J., (1998) "UV microstereolithography system that uses spatial light modulator technology", *Applied Optics, Vol 37 No 32, pp. 7514-22*.

Bertsch A., Bernhard P., Vogt C., Renaud P., 2000, "Rapid prototyping of small size objects", *Rapid Prototyping Journal, Vol. 6, Number 4, pp. 259-266.*

Erdmann L., Deparnay A., Maschke G., Längle M., Bruner R., (2005) "MOEMS-based lithography for the fabrication of micro-optical components", *Journal of Microlithography, Microfabrication, Microsystems. Vol. 4(4), pp. 041601-1, -5.*

Farsari M., Claret-Tournier F., Huang S., Chatwin C., Budgett D., Birch P., Young R., Richardson J., (2000) "A novel high-accuracy microstereolithography method employing an adaptive electro-optic mask", *Journal of Material Processing Technology Vol 107, pp. 167-172.*

Hadipoespito G., Yang Y., Choi H., Ning G., Li X., (2003) "Digital Micromirror device based microstereolithography for micro structures of transparent photopolymer and nanocomposites", *Proceedings of the 14th Solid Freeform Fabrication Symposium, Austin Texas, pp. 13-24.*

Jacobs, P. 1992. Rapid Prototyping and Manufacturing: Fundamentals of StereoLithography. *Society of Manufacturing Engineers.*

Limaye A., Rosen D. 2004. Quantifying dimensional accuracy of a Mask Projection Micro Stereolithography System. *Proceedings of the 15th Solid Freeform Fabrication Symposium, Austin Texas: 481-492*

Limaye, A and Rosen, D 2007. Process planning method for mask projection micro-stereolithography, *Rapid Prototyping Journal 13(2): 76-84*

Mizukami Y., Rajnaik D., Rajnaik A., Nishimura M. (2002) "A novel microchip for capillary electrophoresis with acrylic microchannel fabricated on photosensor array", *Sensors and Actuators B, Vol. 81, pp. 202-209.*

Monneret S., Loubere V., Corbel S., (1999) "Microstereolithography using dynamic mask generator and a non-coherent visible light source", *Proc. SPIE, Vol 3680, pp. 553-561.*

Sager, B.,and D. W. Rosen (2008). "Use of Parameter Estimation for Stereolithography Surface Finish Improvement." *Rapid Prototyping Journal Vol 14, 213-220.*

Sun C., Fang N., Wu D.M., Zhang X., (2005) "Projection micro-stereolithography using digital micro-mirror dynamic mask", *Sensors and Actuators A, Vol. 121, pp. 113-120.*

Referred website: http://www.envisiontec.de; visited on 7th July, 2008.